Appl Compos Mater (2014) 21:707–724
DOI 10.1007/s10443-013-9368-x

Comparison between the Classic Sensor Embedding Method and the Monitoring Patch Embedding Method for Composites Instrumentation

M. Torres · F. Collombet · B. Douchin · L. Crouzeix · Y-H. Grunevald

Received: 1 October 2013 / Accepted: 25 November 2013 / Published online 13 December 2013

Abstract In this paper, the classic embedding technique, with bared sensors, and a recent proposal, the monitoring patch, are compared with the aim to improve the composites in-core instrumentation. The monitoring patch emerges with the need to industrialize sensors integration inside composite structures; thus, a complete evaluation of its mechanical performance has to be done. Numerical and experimental campaigns are carried out on elementary carbon-epoxy coupons to evaluate the benefits and disadvantages of this procedure compared with the typical interlayer sensor embedding. The results show that the use of monitoring patch does not affect significantly the mechanical performance of instrumented coupons. An instrumentation transfer function (ITF) is proposed to link the information that electronic devices can detect, the mechanical phenomena around these electronic devices and the measurements data acquired by global or local techniques (DIC, FEM, gauges). A good correlation between the strain data acquired and the strain values calculated by FEM confirms the approach of the ITF to evaluate the influence of the monitoring patch on the measured signal.

Keywords Composite · Embedding · Bared sensor · Monitoring patch · In-core instrumentation

M. Torres (✉) · F. Collombet · B. Douchin · L. Crouzeix
INSA, UPS, ICA (Institut Clément Ader), Université de Toulouse, 133 C Av. de Rangueil, 31077 Toulouse, France
e-mail: maothor@gmail.com

M. Torres
e-mail: mtorresar@ipn.mx

M. Torres
ESIME Ticomán, Instituto Politécnico Nacional, Av. Ticomán 600, C.P. 07340 México D.F, México

Y.-H. Grunevald
Composites, Expertise & Solutions, 4 Rue Georges Vallerey, 31320 Castanet Tolosan, France

1 Introduction

Composites instrumentation is an emergent domain, because it is not used on industrial structures and it has the potential to cover multiple applications. This approach stands on the information recovered at any given time by several sensors placed in-core and/or at the surface. The collected data are treated in order to establish a link between the sensors' response and the physical state of the composite structure. However, this attachment stays as an open problem and a scientific challenge, which many researchers have shown interest on [1–5].

Composite's instrumentation finds several drawbacks not only on the technical or economical aspects but also on the ideological one, which retards its direct application on industrial structures. One major drawback is the difficulty to obtain information truly representative of the composite's integrity. Another reason why embedded sensors are not widely used is because they are not inherently fail-safe. That is, if the sensor or it connections to the recording instrumentation fail, the monitoring device will most likely assume that the lack of a signal means nothing is happening. Also, it is necessary to conceive the instrumentation process from the very beginning of structure's design, a practice which is not classical today. Additionally, designers frequently assume that the embedded sensor can be the initiation site for delamination growth. Therefore, the sensor is assumed to be an implanted flaw. Finally, the sensors' wire connection creates a constraint for signal recovery and for its replacement in case of miscarriage [6, 7].

Hundreds of academic and industrial teams have worked on this domain worldwide more than 20 years. Some institutions, like NASA have important scientific resources that regroup scientific transverse capabilities such as sensors, signal treatment, composite structures and embedded systems.

Additionally, multiple physical principles, like optical signals, PZT and MEMS, have been imagined to develop numerous innovating sensors' prototypes. Some of these devices are glued on surface, while others are in-core embedded. In laboratory and on test cases, they are currently capable to deliver information of the creation and the evolution of degradation mechanisms or damage [8, 9].

The number of composite industrial structures on transport domain, and particularly on aeronautics and space, is infinity. For these applications, the failure probability of structural components is commonly fixed at 10^{-9} by flight hour. Therefore, it should be convenient to demonstrate that the chain damage - sensor - signal treatment - decision taking presents a failure probability widely smaller, like 10^{-11} by flight hour [10, 11].

This background suggests working on numerical models of thermomechanical behaviour that integrate the structure's reality, and therefore its variability. Also, these models should define pertinent target marks that regroup the physical behaviour at the different scales of the composite structure.

The sensors development has to be done in two ways. On one hand, the devices should translate the evolution of the targets marks, and on the other hand, they should coexist without causing any influence over the structural health integrity. Additionally, this process must be carried out with a limited number of sensors capable to cover extended surfaces. Nowadays, we don't know how to link on a direct way the information delivered by the sensor and the real state of the composite structure. In fact, the sensors must resist severe manufacturing conditions like temperatures up to 180 °C and pressures over 7 bar [12–14, 28–32]. Therefore the sensors' should be integrated on the manufacturing process without additional tasks on it. During the composite structure manufacturing, the sensors should record several parameters in order to allow the definition of the initial state, which is a function of the internal stresses and strains. Each sensor must be replaceable after a local damage on the structure or a proper

malfunction. That is why the reparability constraints should be taken into account in the sensors' design process.

Fibre Bragg Gratings (FBG) is the most common sensors to be used for composites in-core instrumentation. Their long fibre morphology gives them plenty adaptability to identify strains and temperature changes inside composite structures [1, 2, 4–6, 9, 11–13, 29, 30]. Nonetheless, there are some physical phenomena applications such as identification of internal damage or damping where FBG do not give direct measurements. In this case, it is necessary to use another kind of sensors that can detect these phenomena inside composite structures. This is the reason why "ceramics sensors" are an attractive alternative to researchers all over the world [3, 7, 8, 10, 15–21].

Composites instrumentation with ceramic sensors is visualized typically by placing the devices directly between the composite plies during the lay-up. Nonetheless, the sensor's addition creates geometric and material discontinuities inside the composite structure. With this distortion, the stress flux inside the instrumented structure is locally modified with the risk to create an interior damage.

Several studies have analysed the mechanical performances of composite structures instrumented with PZT devices [16–21]. From the late 1990's, there was an interest to evaluate different forms of sensor's placement such as ply embedding or ply cut-out embedding. These first thoughts to conceive sensor housings inside composite structures were proposed at the same time [21, 22]. A proposition for hosting the sensor with grouped or dispersed plies interlacing gave the composite coupons a better performance to crack propagation. However, even when there was not a remarkable influence on the mechanical properties due to the sensor's presence, there was not concluding evidence if the initial damage was caused by the embedding procedure or the sensor's housing [21–25].

Because the sensor housings studied before are built in the structure itself, they cause perturbations on the sensor's neighbourhood such as resin pockets or plies misalignments. These perturbations are a big unknown since it is not possible to make a clear definition of the sensor surroundings. Also they could influence the sensors response, or moreover, they could create the very first damage to the structure. These perturbations, near the bared sensors, remain few studied until now and could become a major risk for the integrity of the composite structure.

For this reason, the ICA and CES Company propose an alternative technique of sensor's embedding for composite structures: "the monitoring patch" [3]. This methodology is conceived to promote composite instrumentation into industrial level, particularly by granting the consistency of the industrial chain. The monitoring patch is based on the idea of minimizing sensors intrusion effect by governing their integration, by controlling the environment which surrounds the sensor.

The embedding method by monitoring patch is easier to integrate on the structure by its dimension on centimetres, without extending considerably the manufacturing procedure of the composite structure. The in-core sensor insertion is more automatic than the insertion of sensors of very tiny dimensions. Furthermore, the monitoring patch has a mechanical and electrical protection role on the sensor. This property allows an improvement on the measurement capability which at least should be at the same range than the trustworthiness of the instrumented structure. This embedding technique can be applied to multiple technologies such as PZT [7, 8, 16–19, 32] or flexible ultrasonic transducers [14, 32]. A similar approach to the monitoring patch has been suggested for tracking crack growth in metallic structures. It is call a crack growth gage [2] and it has been used to track damage accrual in plane stress aircraft structures. However, the difference with the crack growth gage relays on the valued added that monitoring patch will give to composites as in-core instrumentation embedding technique.

To quantify the benefits of the monitoring patch, it is necessary to compare it with the classic embedding technique. The first paper treating the feasibility of monitoring patch had shown promising results [3]. However multiple opened questions about the mechanical performances of composite structures instrumented by this proposal came through.

On the scope of this research, the manuscript is ordered as follows. First, an experimental set-up is briefly described in order to compare three groups of epoxy carbon coupons: one without instrumentation, one with in-core bared sensors and one with the monitoring patch. Then the results are compared by means of Digital Image Correlation and FEM models. The analysis of in-core strains (those that sensors could acquire) and out-side strains (those recovered by DIC or strain gauges) is discussed by means of an instrumentation transfer function. Finally, the concluding remarks are cited to expose the benefits and drawbacks of the monitoring patch as instrumentation technique.

2 Experimental Procedures

2.1 Tensile and Four-Point Bending Setups

In order to show the advantages and disadvantages of monitoring patch face to the classic embedding procedure, a comparison by an experimental-numerical campaign is done. The sensor intrusiveness is seen from a numerical point of view. Then, the concept of transfer function is presented here to quantify the influence of the patch and is value added.

Three sets of Hexcel M21 T700 GC carbon-epoxy coupons were fabricated via autoclave. The first group consists in free-sensor coupons which are used as reference. Then, the second group includes coupons with a bared sensor between the composite plies. Finally, the third group involves coupons with a monitoring patch inside. All groups have three coupons each one, in order to have reliable statistical results.

On this work, the mechanical comparison is the priority; therefore, polycrystalline silicon lures are used as sensors. These silicon lures are used as main ceramic substrate for tunnelling junction sensors (TJS) developed by LAAS [32]. The size of these decoy sensors is fixed on $2\times2\times0.3$ mm and they are glued to a PCB Kapton flex connection of 50 mm long. The monitoring patch consists in four CTMI pre-impregnate epoxy/glass plies, as described in [3]. The decoy sensor is placed over a base ply, followed by two hosting plies and finishing with a covering ply, giving the patch 55 mm per side. The strategy chosen here cannot take advantage of in-situ measurements. On one hand, the sensors employed are mute, and on the other hand, the evaluation method for the monitoring patch must be established whatever the use of the sensor. The goal is to link a surface measurement with in-core information calculated by numerical simulations. This goal is inducted under two loading configurations: traction and bending. For the tensile tests, the following eight plies quasi-isotropic configuration is selected: (0/45/90/-45/bared sensor or patch/-45/90/45/0). The monitoring patch is placed on the middle plane of the tensile coupons. For the bending tests, the following seventeen plies quasi-isotropic configuration is proposed: (0/45/90/-45/0/-45/90/45/0/45/90/-45/0/-45/90/bared sensor or patch/45/0). The monitoring patch is placed outside the middle plane of the bending coupons. Figure 1 shows the two types of instrumentation, bared sensor and monitoring patch during coupons manufacturing process.

Due to the loading capacity of the testing machine, the nominal dimensions for the carbon-epoxy coupons are $300\times75\times2$ mm with a testing zone restricted to 200 mm. For the coupons instrumented with the monitoring patch, the patch-coupon width ratio is 0.6 [3]. All specimens are instrumented with strain gauges at the surface: one gauge at the sensor's location and one

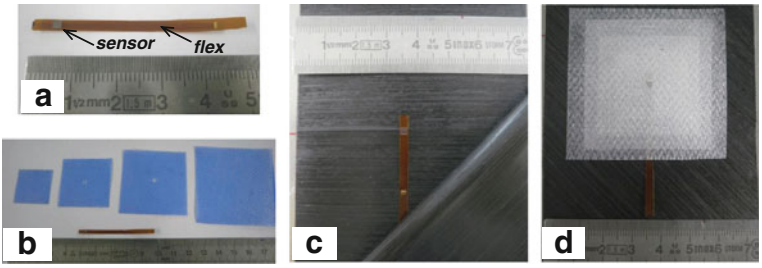

Fig. 1 Manfacturing of carbon-epoxy coupons for in-core instrumentation. **a** Sensor with flex connexion, **b** constitutive plies of monitoring patch, **c** coupon with bare sensor and **d** coupon with monitoring patch

gauge at the flex connection end. For coupons with monitoring patch an additional gauge at the patch border is placed. All mechanical tests are carried out at a displacement rate of 2 mm/min until the coupon failure is reached.

Coupons for tensile tests are painted with a black/white random speckle pattern in order to record them with Digital Image Correlation (DIC) [26, 27]. This time, a pair of 8-bit Qimaging Qicam CCD cameras, with 2.4 mm diameter Tamrom lenses and 70 mm of focal distance, is used. The region of interest (ROI) is fixed on the instrumented zone, with a bared sensor or a monitoring patch, in order to acquire the displacements due to the imposed loading. During the tensile tests, an image is taken every 3 kN. Image post-treatment is done by means of the VIC 3D® software. Image resolution is $1{,}360 \times 1{,}036$ px^2 with a subset (S) of 19×19 px^2 and a step (p) of 9 px. The image resolution (g) is estimated to be 0.11 mm/px and the spatial resolution (S·g) is calculated in 2.1 mm.

For the 4-points bending tests, the support span is fixed on 200 mm while the loading span is established in 100 mm. The instrumented zone, with bared sensor or patch, is placed on the extended face during the test. Figure 2 illustrates the experimental setup for the tensile and four-point bending tests.

2.2 Numerical FEM Models

With the goal to complete an experimental-computational study two numerical models are performed using the finite element method (FEM) by means of the SAMCEF™ software. The 2D model is created with 16640 linear multilayer shell elements and 50177 nodes (cf. Fig. 3a). The boundary conditions for the tensile test are described as follows. The model is clamped at the bottom by means of the fixations along the X, Y, and Z axes and fixing also the rotation along Y axis. At the top, the fixations are set along the Y and Z axes. The machine

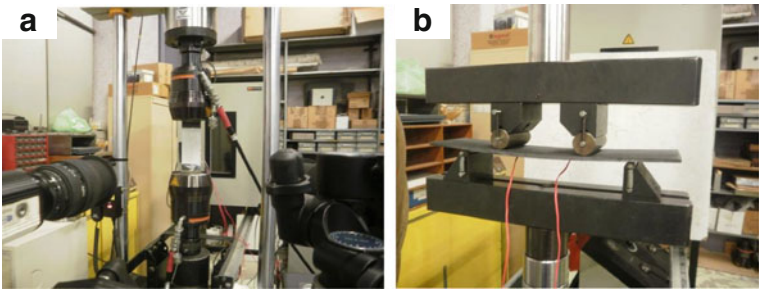

Fig. 2 Experimental setup for the instrumented coupons, **a** tensile test with DIC and **b** 4-point bending test

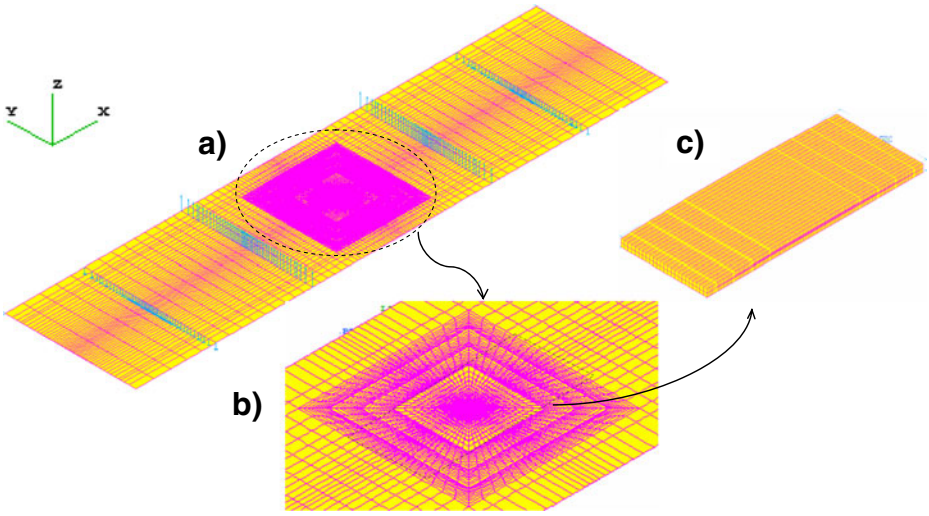

Fig. 3 FEM models developed for the comparison between the two embedding techniques: **a** 2D model of the 4-point bending test, **b** numerical zoom of the 2D model and **c** 3D model of the instrumented zone

displacement is imposed via the X direction. On the other hand, boundary conditions for the four-point bending test are the following. On the support lines, the translation on Z axis remains blocked. The machine displacement is imposed on the Z direction on the loading lines. This simple modelling is acceptable because of the distance between the studied zone and the boundary conditions imposed to the specimen.

The 3D model is proposed to represent the constitutive lay-up at the instrumented zone with a better precision. The use of a 3D model lies on study the delamination and interlaminar fracture on the instrumented zone in further works. This model, at the mesoscopic scale, is created with 20833 linear multilayer cubic elements and 73530 nodes. For the instrumented structure, each element through-the-thickness represents four carbon-epoxy plies. In the case of the monitoring patch, each element through-the-thickness represents a glass-epoxy ply of the patch. Resin pockets at the corners of patch plies are simply modelled with tetrahedral isotropic elements. The boundary conditions are obtained from the results calculated by the 2D model and used at the edge of the instrumented zone. For the tensile test, the average value of the displacement field on the patch border at the mobile clamp is recovered. Then, these values are imposed on one edge of the 3D model; meanwhile, the other edge is clamped with the same restrictions described for the 2D model. For the bending test, the average deflection displacement on the instrumented zone is obtained. Then, the displacement values are imposed along the middle plane of the 3D model and the edges are simply supported like the 2D model. Illustrations of the 2D and 3D models are shown in Fig. 3.

3 Comparison Between Bared Sensor and Monitoring Patch Instrumentations

3.1 Coupons Tested Under Tensile Loading

The mechanical response of carbon-epoxy coupons under tensile loading is described by means of load – strain curves. Strain values obtained by each method, strain gauges, DIC and FEM models are compared.

First, there is interest to set the initial state on the instrumented zone surface for the three kinds of coupons. Figure 4 presents the topographic field acquired by the CCD cameras for the reference, bared sensor and monitoring patch coupons. For the reference coupons, there is homogeneity on the surface heights; therefore, the thickness remains constant. For the bared sensor coupons, the heights champ reveals the presence of the sensor and its flex connection. A small protuberance is created due to the sensor and numerous height irregularities are visible. These random defects are possibly related to the classical embedding process. For the monitoring patch coupons, the image shows a considerable hump caused by the embedded patch. However, the monitoring patch guarantees a gradual change on the coupons thickness. The surface out of the monitoring patch is more regular, which describes uniform sensor integration with the structure and more control on the embedding process.

For the tensile tests, Fig. 5 shows the load – strain curves for the three types of coupons. Even if all coupons have a linear behaviour, the measurements obtained on sensor's location show some differences for each kind of coupons. The reference coupons and the bared sensor coupons have a larger elongation than those with the monitoring patch. The monitoring patch coupons seem to be the most stiffened of the three types. The three types of coupons present the same strength level. If we are interested on the local stiffness at sensor's location, the coupons provided with a monitoring patch are 10 % more stiffened than those with a bared sensor inside and 20 % more stiffened than the reference coupons. This behaviour is expected, from a qualitative point of view, because of the local over-thickness caused by the monitoring patch.

As a visual support, Fig. 6 shows the longitudinal strain field (ε_{xx}) by DIC for each family of coupons: reference, with bared sensor and with monitoring patch. The longitudinal strain field for the reference coupons and those with bared sensor do not reveal substantial differences. It is hard to conclude that fracture of bared sensor coupons occurs due to imposed load or due to the presence of the sensor; nonetheless, the main crack is near to sensor's location. For the coupons equipped with a monitoring patch, the longitudinal strain field (ε_{xx}) is heterogeneous and reveals particular zones. The patch zone presents the lowest strain values for the entire cartography. Strain rises gradually from sensor's emplacement until the patch borders. The patch borders show over-strained zones which reach the coupon's edges. It is

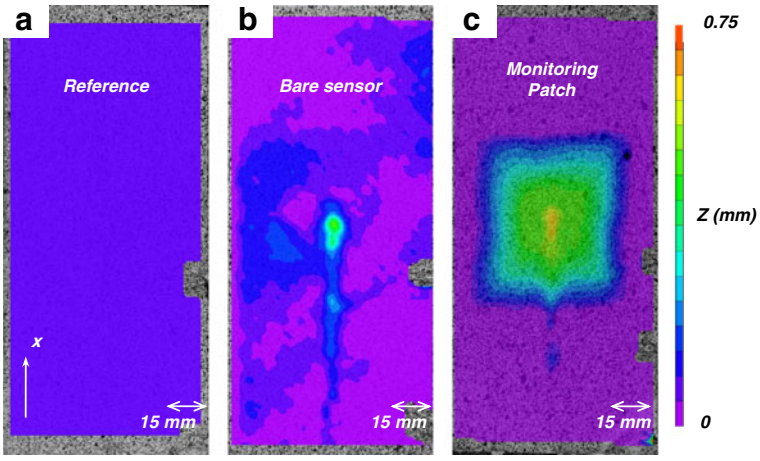

Fig. 4 Topographic fields for the three types of coupons **a** reference coupons, **b** coupons with bare sensor and **c** coupons with monitoring patch

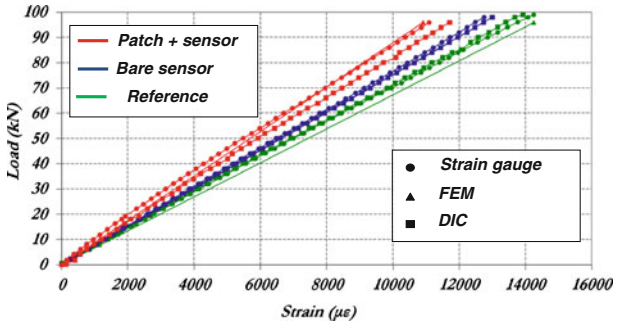

Fig. 5 Load – longitudinal strain (ε_{xx}) curves comparing the three types of instrumented coupons under tensile loading

important to remark that the main crack on this kind of coupons is localized on the patch border, causing the final failure of the composite coupon.

Whatever the embedding technique employed, the sensor creates an over-thickness which modifies locally the geometry of the composite structure. The over-thickness promotes lower strain values on this zone than the strain mean value for the rest of composite coupon. For coupons with the bared sensor inside, the thickness changes abruptly, however, for coupons with the monitoring patch the over-thickness zone varies regularly thanks to the slope of the monitoring patch constitutive plies. For this reason, the patch edge is under a higher stress state which generates over-strained zones.

Figure 7 shows a qualitative and quantitative comparison between the longitudinal strain field for the monitoring patch coupons by DIC and FEM. A good correlation between experimental and numerical tests in terms of localization and strain intensity can be noticed. Additionally, Fig. 8 shows the strain field at the surface ply (0°) for both FEM models proposed. Both have similar tendencies for the strain cartography and showing the strain field heterogeneity of the instrumented zone by monitoring patch. The goal to make these

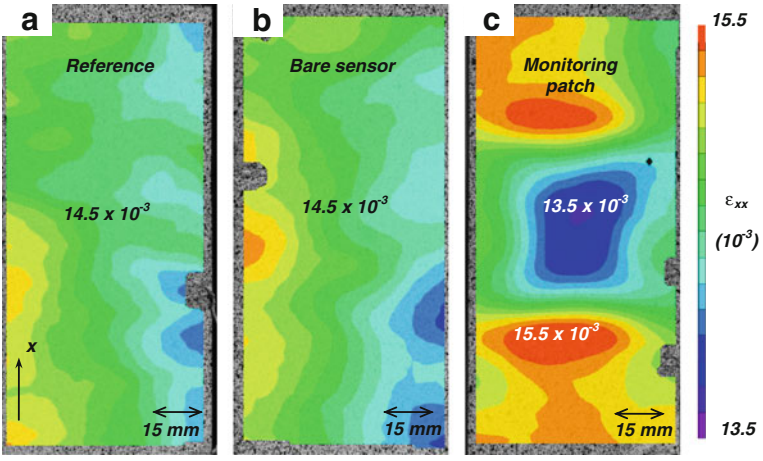

Fig. 6 Longitudinal strain field (ε_{xx}) at the surface ply (0°) before failure (94 kN) for the **a** reference coupons, **b** bare sensor coupons and **c**) coupons with monitoring patch

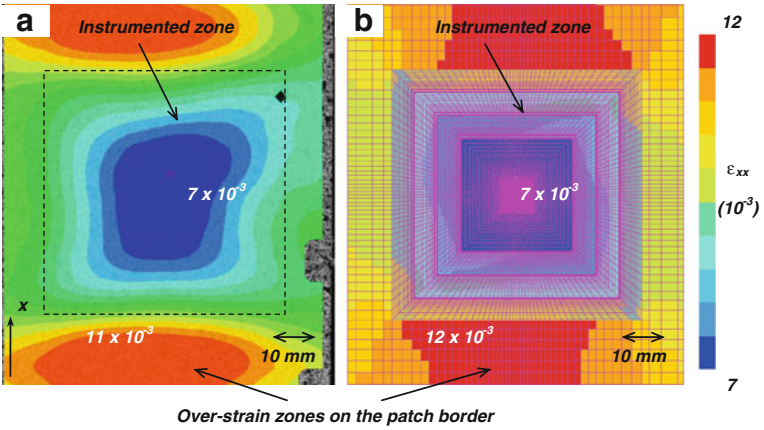

Fig. 7 Longitudinal strain field (ε_{xx}) at the surface ply (0°) for the coupons with monitoring patch by **a** DIC and by **b** FEM for 66 kN of tensile load

qualitative comparisons is to validate the correct convergence of both numerical models and to justify their further use to evaluate the instrumentation transfer function (ITF).

3.2 Coupons Tested Under Bending Loading

An analogous procedure is made to evaluate the mechanical performances of instrumented carbon-epoxy coupons under 4-point bending test. The strain-load curves are plotted with data acquired by two techniques: strain gauges and FEM on Fig. 9. The three types of coupons exhibit linear behaviour at the beginning of the test, followed by non-linear performance at the end of the test. The strain measurements display that instrumented coupons are more stiffened

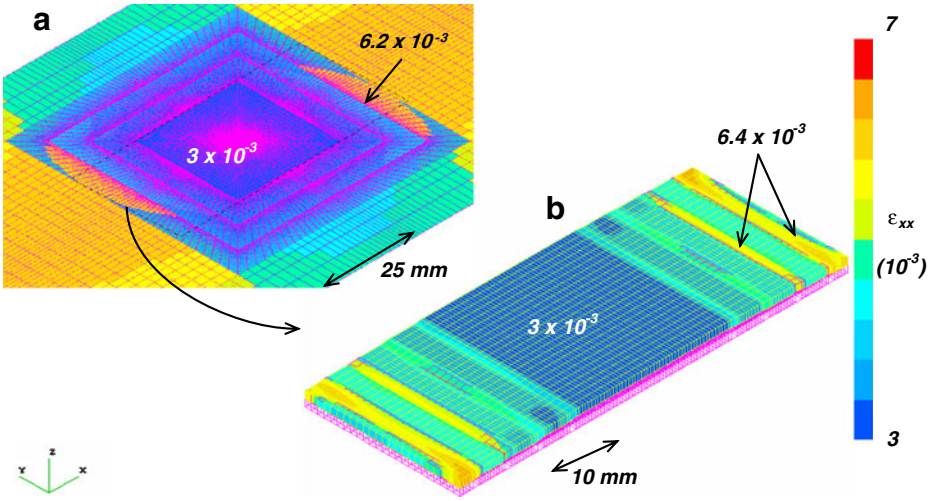

Fig. 8 Longitudinal strain field (ε_{xx}) on the instrumented zone at the surface ply (0°) for 30 kN of tensile load by **a** 2D shell model and **b** 3D tetrahedral model for coupons with monitoring patch

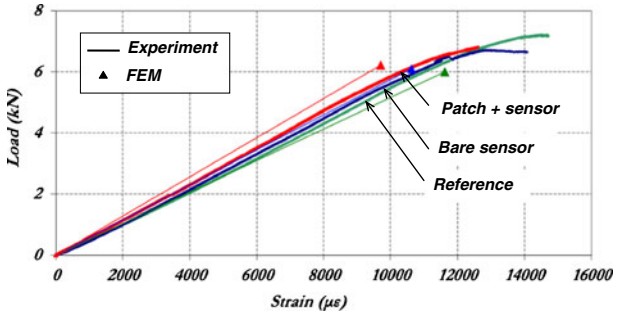

Fig. 9 Load – longitudinal strain (ε_{xx}) curves comparing the three types of instrumented coupons under 4-point bending loading

than reference coupons. Once again, coupons prepared with a monitoring patch seem to be the most stiffened from the three families. All coupons have a similar ultimate strength, nonetheless, on the linear zone the coupons with monitoring patch are almost 10 % more stiffened than coupons with bared sensor and almost 20 % more stiffened than the reference ones.

These observations are verified with the FEM models. Figure 10 illustrates the longitudinal strain field (ε_{xx}), at the surface ply on the bend side, for the coupons with monitoring patch. As well as for the tensile test, the instrumented zone reveals a heterogeneous strain field. The zone of sensor location stays less strained than the patch border, which appears as the most strained zone for the entire coupon. The gap between the strain values for the sensor zone and for the patch border is 15 %. With these results, the patch border is, once again, the zone with the highest risk to crack propagations and possible fractures.

Fracture modes for the instrumented coupons are illustrated in Fig. 11. The most important delamination, for coupons with bared sensor, appears between those plies

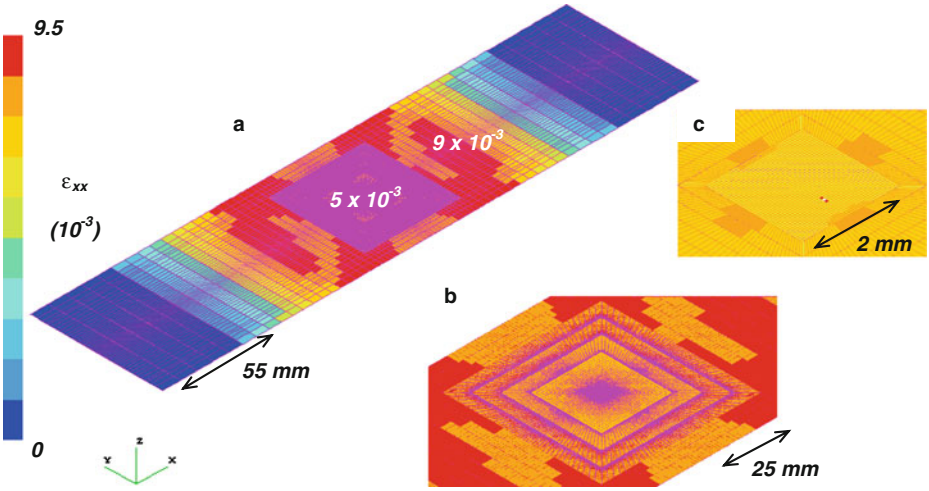

Fig. 10 Longitudinal strain field (ε_{xx}) for the 4-point bending coupon with monitoring patch by FEM models at 3kn load. **a** Strain mapping of the external ply, **b** zoom for the instrumented zone and **c** zoom on the sensor location

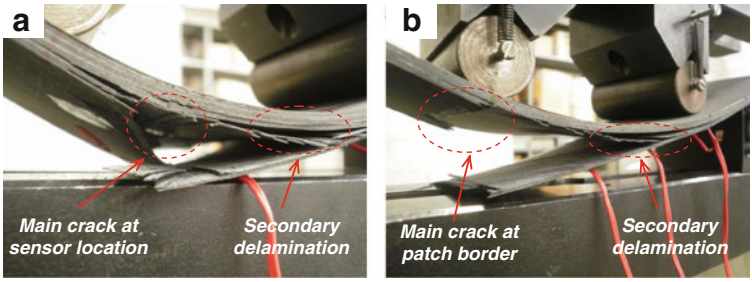

Fig. 11 Illustrations of the final failure of instrumented coupons under 4-point bending test, **a** bare sensor coupon and **b** coupon with monitoring patch

where the device was placed. The interlaminar fracture causes a partial debonding of the sensor and its wire connection from the composite plies. There is also a secondary damage on the interface of the plies below the sensor due to the bending loading. Delamination for coupons with monitoring patch appears on the ply above the monitoring patch. As well as for the tensile test, the main crack is found on the patch border because the instrumented zone is more stiffened due to the presence of the patch. There is too a supplementary damage on the surface plies of the coupons due to the bending load. In both load cases, even if the internal drop-off slope of the patch's plies diminishes the intrusive effect of the sensor, the coupon-patch border seems to be the weakest point for an elementary composite plate instrumented with a monitoring patch.

4 Link Between the Strain Field of Embedded Sensor and Strain Values Measurable on Surface: The Instrumentation Transfer Function

Once the strain field of coupons with monitoring patch is described, the next step is to analyse the strain level to which the sensor stands to. In further work, the strain of the sensor, calculated by FEM will be compared with the information provided by the sensor itself when it is fully operational. With the numerical – measurement correlation cited above, the possibility to link a stimulus captured by the sensor to a mechanical event on the near surroundings should be done with better accuracy.

The link between the strain level to which the sensor stands to (ε_s), the strain mean value of the near surroundings (ε_n) and the strain on surface (ε_{su}) will be know it, from now on, as "instrumentation transfer function (ITF)".

4.1 Instrumentation Transfer Function in Tension

Figure 12 shows the longitudinal strain field for the sensor and its wire connection embedded in the monitoring patch by FEM for the tensile coupons. According to the numerical results, the strain value on the patch base-ply (ε_n) is 20 to 25 % bigger than the strain value recorded on the sensor (ε_s). With this observation, the strain of the near surroundings (ε_n) is partially transmitted through the patch and finally captured by the sensor. Therefore, the strain level detected by the sensor (ε_s) is a function of the strain level at the near surroundings (ε_n), mainly those on the patch

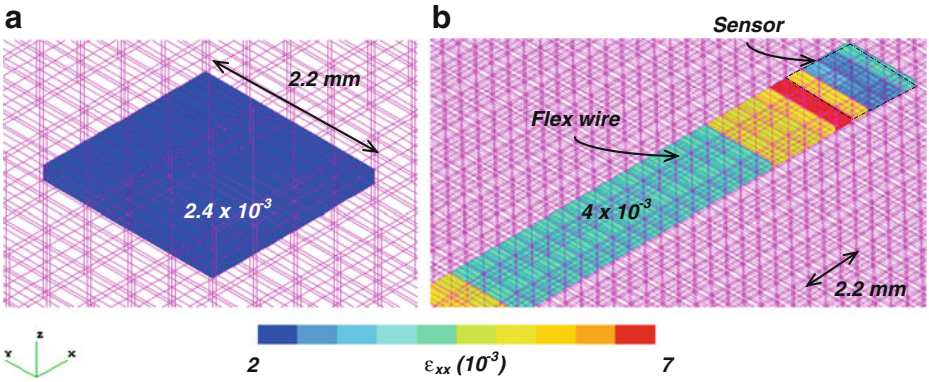

Fig. 12 Longitudinal strain field (ε_{xx}) for **a** the tunnelling junction sensor and for **b** the flex wire connexion by FEM (tensile test at 30 kN)

base-ply. The strain level can be adjusted by a correction factor, called from here now as "encapsulation factor in tension (m_t)". This hypothesis is described in Eq. 1:

$$\varepsilon_n = m_t \cdot \varepsilon_s \quad with \quad 1.2 \leq m_t \leq 1.25 \tag{1}$$

The main consequence of sensor encapsulation is that electronic devices only capture a portion of the strain in the near surroundings. Regardless the embedding technique, this can be due to the difference between the compliance of the sensor's material and its local environment and the compliance associated with the composite structure. For this reason, the encapsulation factor cited before plays a huge role to link the measurements acquisition by the sensors and their correct interpretation.

The strain value at the surface ply, where any other technique can be applied (DIC, strain gauges), is known from now on as "strain on surface (ε_{su})". Figure 13 shows

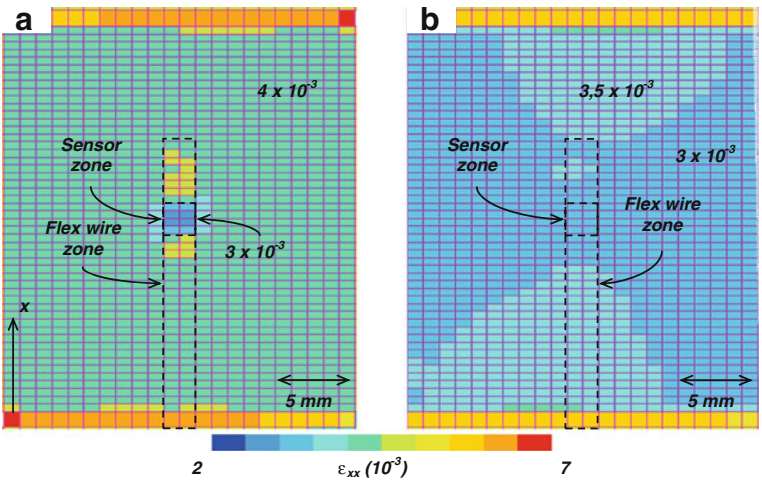

Fig. 13 Longitudinal strain field (ε_{xx}) for **a** the −45° carbon – epoxy ply adjacent to the patch and **b** the 0° carbon – epoxy ply at the surface of the instrumented coupon (bottom view of 3D FEM model, tensile test at 30 kN)

the longitudinal strain field for the near surroundings on the ply at 45° adjacent to the patch and for the ply at 0° at the surface of the composite coupon. Both strain fields are plotted with the 3D FEM model. As well as described before, the sensor strain (ε_s) can be linked with the strain on surface (ε_{su}) to which values could be recovered also through surface techniques (DIC, gauges, etc.). These two values can be adjusted by a correction factor, called "instrumentation factor in tension (n_t)". The mathematical relation now is written in Eq. 2:

$$\varepsilon_{su} = n_t \cdot \varepsilon_s \tag{2}$$

On the case of tensile tests, all the plies inside de coupons are under the same range of global strain. In consequence, the near surrounding strain (ε_n) is equal to the strain on surface (ε_{su}). The encapsulation factor in tension (m_t) is therefore equal to the instrumentation factor in tension (n_t). With this axiom (cf. Eq. 3), there is now a real possibility to compare the internal strains of a composite structure with the external measurements that are available with different global and local technologies. In this context, the relation between information from many sources must be correlated and corrected with the factors cited above to assure a credible interpretation.

$$\begin{aligned} \varepsilon_{su} &= \varepsilon_n \quad \Rightarrow \quad m_t = n_t \\ \varepsilon_{su} &= m_t \cdot \varepsilon_s \quad \textit{for tensile tests} \end{aligned} \tag{3}$$

Figure 14 shows at two loading stages on the tensile tests, the strain values for the different zones acquired or calculated by the experimental and numerical techniques described previously. The monitoring patch is able to transfer between 80 % and 85 % of the strain in the near surroundings (ε_n) toward the sensor. In one hand, we assume that this information should be enough accurate to determine the strain amplitude on the zone that needs constant monitoring. In the other hand, this attenuation effect protects the sensor which can operate up to the damage of the zone of interest, for example, in the case where the maximum admissible strain of the sensor is lower than the strain of the monitored zone. Equation 3 has resumed the instrumentation transfer function (ITF) for composite coupons with monitoring patch under tensile load.

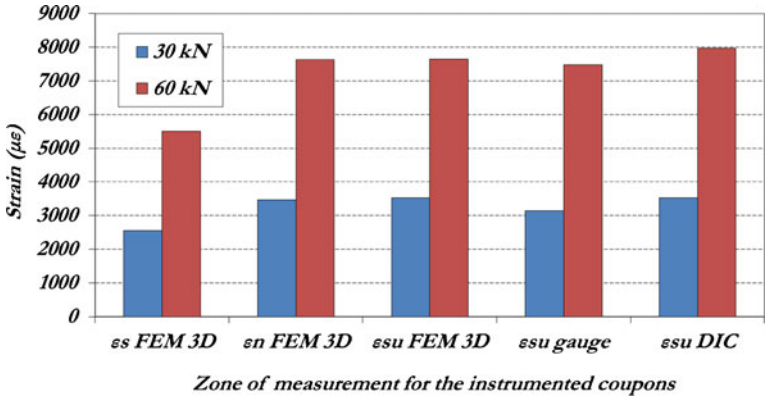

Fig. 14 Comparison between the strain mean values on the different target zones of coupons with monitoring patch by different measurement techniques for the tensile test

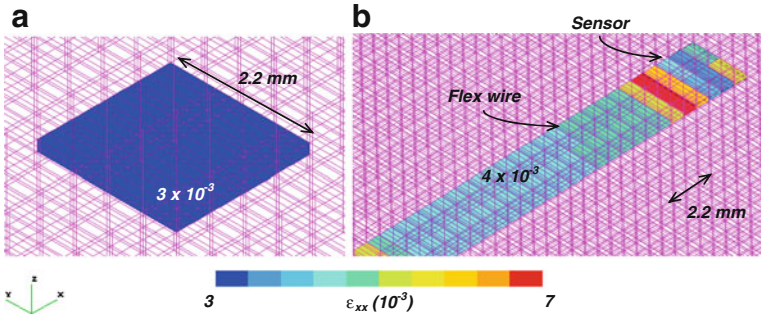

Fig. 15 Longitudinal strain field (ε_{xx}) for **a** the tunnelling junction sensor and for **b** the flex wire connexion by FEM (4-point bending test at 3 kN)

4.2 Instrumentation Transfer Function in Bending

We proceed in a similar way, in order to establish the influence of instrumentation in composite coupons under 4-point bending condition. Same consideration used before is taken; both the patch base-ply and the carbon-epoxy ply adjacent to it have the same strain level. The numerical results show that the near surrounding strain (ε_n) is 20 to 25 % higher than the sensor strain (ε_s), as shown in Eq. 4. With this fact, it can be stated that the "encapsulation factor in bending (m_b)" stays at the same range for the two loading conditions imposed.

$$\varepsilon_n = m_b \cdot \varepsilon_s \quad with \quad 1.2 \leq m_b \leq 1.25 \quad \Rightarrow \quad m_t = m_b \tag{4}$$

On one hand, Fig. 15 shows the longitudinal strain field for the sensor and its flex connection embedded in the monitoring patch by FEM for the 4-point bending coupons. On the other hand, Fig. 16 illustrates the longitudinal strain field for the near surroundings on the ply at 90° adjacent to the patch and for the ply at 0° at the

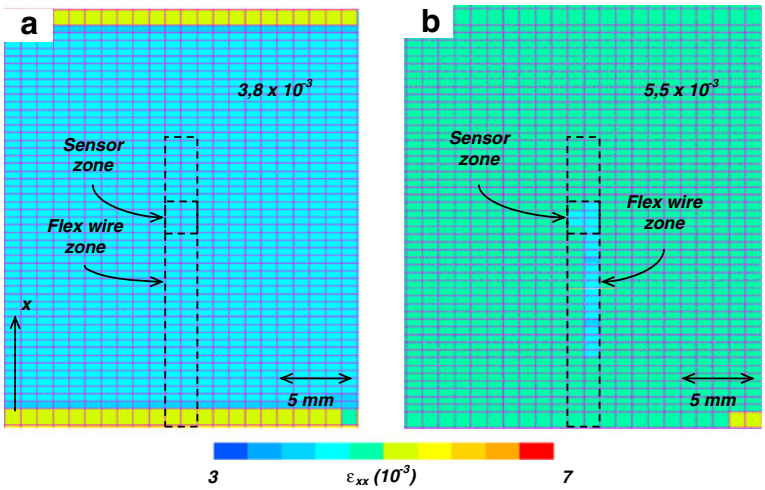

Fig. 16 Longitudinal strain field (ε_{xx}) for **a** the 90° carbon – epoxy ply adjacent to the patch and **b** the 0° carbon – epoxy ply at the surface of the instrumented coupon (bottom view of 3D FEM model, 4-point bending test at 3 kN)

bend surface of the composite coupon. Both strain fields are plotted with the 3D FEM model as well.

The strain level changes from ply to ply through-the-thickness on a 4-point bending plate. The strain becomes zero if we approach to the neutral fibre and raises the highest values if we are near the external plies. If the monitoring patch is placed on the coupons surface, the near surroundings strain (ε_n) and the strain on surface (ε_{su}) will have the same value. However, if the patch is embedded, the near surroundings strain will be proportional to the distance which separates the adjacent ply to the patch with the neutral fibre of the plate. The relation between (ε_n) and (ε_{su}) now is depicted in Eq. 5:

$$\varepsilon_n = \frac{2d}{e_p} \cdot \varepsilon_{su} \quad with \quad 0 < \frac{2d}{e_p} \leq 1 \tag{5}$$

Where d is the distance from the neutral fibre to the position of the patch base-ply and e_p is the thickness of the composite plate.

Going back to the definition of near surroundings strain (ε_n), the strain on surface can be written as a function of the sensor strain (ε_s). Equation 6 describes this relation as follows:

$$\varepsilon_n = m_b \cdot \varepsilon_s \quad ; \quad \varepsilon_n = \frac{2d}{e_p} \cdot \varepsilon_{su} \quad \Rightarrow \quad \varepsilon_{su} = \frac{m_b \ e_p}{2d} \cdot \varepsilon_s \tag{6}$$

Finally it can be attested that the instrumentation factor in bending (n_b) depends on the encapsulation factor (m_b) and also on the location of the monitoring patch inside the composite plate. Equation 7 describes this conclusion:

$$\varepsilon_{su} = n_b \cdot \varepsilon_s \quad with \quad n_b = \frac{m_b \ e_p}{2d} \tag{7}$$

For this reason the numerical results, for the 4-point bending coupons, show that the strain on surface (ε_{su}) is up to 70 % higher than the sensor strain (ε_s). The correct interpretation of the data acquired by the sensor will depend on the embedding technique, in this case due to the monitoring patch. The relevant comparison showed here is between the data acquired by the decoy sensor and the data measured at the surface.

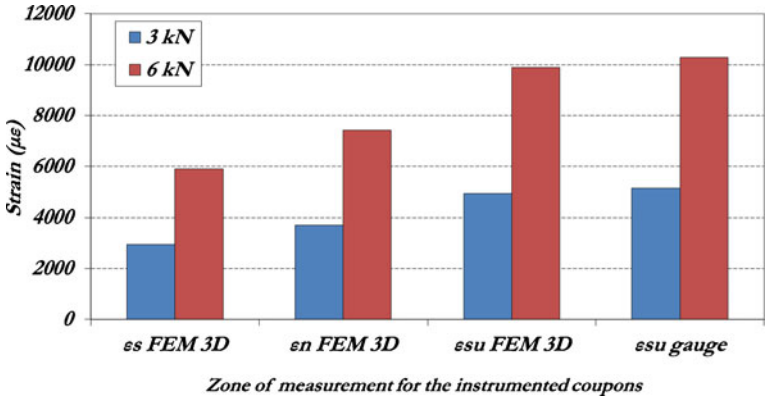

Fig. 17 Comparison between the strain mean values on the different target zones of coupons with monitoring patch by different measurement techniques for the 4-point bending test

Figure 17 displays for two loading stages for the 4-point bending tests, the strain values for the different zones acquired or calculated by all the experimental and numerical techniques described earlier. The variation on the strain values confirms that the information that the sensor receives has to be adjusted with the instrumentation factor in order to compare it with the acquisitions on the zone of interest. At the end, Eq. 7 has described the instrumentation transfer function (ITF) for composite coupons with monitoring patch under bending load.

5 Conclusions

On the scope of this article, a comparison between the classic embedding technique and another by monitoring patch is done in order to evaluate this new proposal for the instrumentation of composite structures.

Carbon – epoxy coupons with embedded instrumentation, bared sensors and monitoring patch, are tested under tension and 4-point bending to determine their mechanical performance. Strain fields for each type of coupons are quantified with local techniques (gauges) and global procedures (DIC and FEM).

For the classic instrumentation, the mechanical performance of elementary coupons is not affected by the embedded bared sensor. It is difficult to know if the fracture is induced by the value of the imposed loading or by the local distortion generated by the bared sensor. Nonetheless, the main crack is very close to the sensor location.

For the monitoring patch instrumentation, the mechanical performance of elementary coupons is not reduced due to the presence of the monitoring patch. Locally, on the sensor location, these coupons are 10 % more stiffened than those with the classic embedding. The monitoring patch modifies locally the strain field by creating over-strained zones at the patch border. At this site, the coupons appear to be more vulnerable to crack initiation and failure propagation.

From the fact that the sensitive face of the sensor is always en contact with the patch base-ply, the sensor is more stimulated by the strains of this layer. The numerical models show that the strain level of the sensor's nearest carbon-epoxy ply is similar to the strain level of the patch base-ply. With these results, the monitoring patch assures the good strain transfer between the composite structural layers and the sensor device.

On this paper, the instrumentation transfer function (ITF) is proposed to relate the strain level of the sensor (ε_s), the value of the near surroundings strain (ε_n) and the strain on surface (ε_{su}). The ITF relays on the sensor's encapsulation factor (m). The correction factor of the data acquired by the sensor will depend on the use of the monitoring patch as embedding technique.

All tested made show the viability to instrument elementary composite coupons with the monitoring patch. The monitoring patch has the potential to be applied on piping, civil engineering structures and off-shore installations, where the size, type and connectivity of the sensors have not severe restrictions. The very next step is to apply the monitoring patch in the scope of a Multi-Instrumented Technical Evaluator (MITE) [28] to evaluate composite structures from their manufacturing [29–32] until their service under combined loadings. However, further work should continue the exploration of this proposal in order to apply it on the framework of industrial scale structures.

Acknowledgments The present work is part of the research project "Multi-sensor Instrumentation for Composite Materials and Structures (I2MC)" financially supported by the Thematic Advanced Research Network for

Aeronautic and Space Sciences & Technologies of Toulouse (RTRA STAE). The first author conveys his special appreciation to the National Council of Science and Technology of Mexico (CONACYT) for the financial support.

References

1. Baker, W., McKenzie, I., Jones, R.: Development of life extension strategies for Australian military aircrafts using structural health monitoring of composite repair joints. Compos. Struct. **66**, 133–143 (2004)
2. Baker,: Structural health monitoring of a bonded composite patch repair on a ratigue-cracked F-111C wing. Air Vehicles Division, Defence Science and Technology Organisation, DSTO-RR-0335, Australian Government (2008)
3. Torres, M., Crouzeix, L., Collombet, F., Douchin, B., Grunevald, Y.-H.: Mechanical characterization of an alternative technique to embed sensors in composite structures: the monitoring patch. Appl. Compos. Mater. **19**, 379–391 (2012)
4. Luyckx, G., Voet, E., Geernaert, T., Chah, K., et al.: Response of FBGs in microstructured and bow tie fibers embedded in laminated composite. IEEE Photon. Technol. Lett. **21**(18), 1290–1292 (2009)
5. Collombet, F., Mulle, M., Grunevald, Y.H., Zitoune, R.: Contribution of the embedded optical fiber with Bragg grating in composite structures for tests-simulations dialogue. Mech. Adv. Mater. Struct. **13**, 429–439 (2006)
6. Hernández, H., Collombet, F., Douchin, B., Choqueuse, D., Davies, P., González, J.L.: Entire life time monitoring of filament wound composite cylinders using Bragg grating sensors: I. Adapted tooling and instrumented specimen. Appl. Compos. Mater. Struct. **16**(3), 173–182 (2009)
7. Su, Z., Wang, X., Chen, Z., Ye, L., Wang, D.: A built-in active sensor network for health monitoring of composite structures. Smart Mater. Struct. **15**, 1939–1949 (2006)
8. Yan, Y., Yam, L.H.: Online detection of crack damage in composite plates using embedded piezoelectric actuators/sensors and wavelet analysis. Compos. Struct. **58**, 29–38 (2002)
9. Mulle, M, Zitoune, R, Collombet, F.: Through-the-thickness material properties identification in a technological specimen using 3D-DIC and embedded FBG measurements. Exp. Mech. 1340–1343 (2008)
10. Grondel, S., Assaad, J., Delebarre, C., Moulin, E.: Health monitoring of a composite wingbox structure. Ultrason. **42**, 819–824 (2004)
11. Mueller, I., Chang, F.K., Roy, S., Mittal, M., Lonkar, K., Larrosa, C.: A robust structural health monitoring technique for airframe structures. Proceedings of the "7th International Workshop on Structural Health Monitoring" (2009)
12. Mulle, M., Zitoune, R., Collombet, F., Olivier, P., Grunevald, Y.H.: Thermal expansion of carbon–epoxy laminates measured with embedded FBGS—Comparison with other experimental techniques and numerical simulation. Compos. Part A **38**, 1414–1424 (2007)
13. Hernández, H., Collombet, F., Douchin, B., Choqueuse, D., Davies, P., González, J.L.: Entire life time monitoring of filament wound composite cylinders using Bragg grating sensors: III. In-service external pressure loading. Appl. Compos. Mater. Struct. **16**(3), 135–147 (2009)
14. Hernández, H., Collombet, F., Douchin, B., Choqueuse, D., Davies, P., González, J.L.: Entire life time monitoring of filament wound composite cylinders using Bragg grating sensors: II. Process Monitoring. Appl. Compos. Mater. Struct. **16**(4), 197–209 (2009)
15. Kobayashi, M., Jen, C.K., Bussiere, J.F., Wu, K.T.: High-temperature integrated and flexible ultrasonic transducers for non-destructive testing. NTD & E Int. **42**, 157–161 (2009)
16. Zhou, G., Sim, L.M.: Evaluating damage in a smart composite laminates using embedded EFPI strain sensors. Opt. Lasers Eng. **47**, 1063–1068 (2009)
17. Tadigadapa, S., Mateti, K.: Piezoelectric MEMS sensors: state-of-the-art and perspectives. Meas. Sci. Technol. **20**, 1–30 (2009)
18. Tan, P., Tong, L.: A sensor charge output deviation method for delamination detection using isolated piezoelectric actuator and sensor patches. Compos. Part B **37**, 583–592 (2006)
19. Yocum, M., Abramovich, H., Grunwald, A.: Fully reversed electromechanical behavior of composite laminate with embedded piezoelectric actuator/sensor. Smart Mater. Struct. **12**, 556–564 (2003)
20. Cheng, J., Wu, X., Li, G., Taheri, F., Pang, S.S.: Development of a smart composite pipe joint integrated with piezoelectric layers under tensile loading. Int. J. Solids Struct. **43**, 5370–5385 (2006)
21. Yan, W., Wang, J., Chen, W.Q.: Delamination assessment of a laminated composite beam using distributed piezoelectric sensor/actuator. Smart Mater. Struct. **20**, 12–26 (2011)

22. Mall, S., Coleman, J.M.: Monotonic and fatigue loading behavior of a quasi-isotropic graphite/epoxy laminate embedded with piezoelectric sensors. Smart Mater. Struct. **7**, 822–832 (1998)
23. Mall, S.: Integrity of graphite/epoxy laminate embedded with piezoelectric sensor/actuator under monotonic and fatigue loads. Smart Mater. Struct. **11**, 527–533 (2002)
24. Mall, S., Hsu, T.L.: Electromechanical fatigue behavior of graphite/epoxy laminate embedded with piezoelectric actuator. Smart Mater. Struct. **9**, 78–84 (2000)
25. Hansen, J.P., Vizzini, A.J.: Fatigue response of a host structure with interlaced embedded devices. Intell. Mater. Syst. Struct. **11**, 902–909 (2000)
26. Huang, Y., Nemat-Nasser, S.: Structural integrity of composite laminates with embedded micro-sensors. Sensors Syst. Netw. **65**, 1–5 (2002)
27. Crouzeix, L., Périé, J.N., Collombet, F., Douchin, B.: An orthotropic variant of the equilibrium GAP method applied to the analysis of a biaxial test on a composite material. Compos Part A: Appl Sci Manuf. **40**(11), 1732–1740 (2009)
28. Périé, J.N., Calloch, S., Cluzel, C., Hild, F.: Analysis of a multiaxial test on a C/C composite by using digital image correlation and a damage model. Exp. Mech. **42**, 318–328 (2002)
29. Collombet, F., Grunevald, Y.H., Zitoune, R., Mulle, M.: Economical value added of multi instrumented technological evaluators for the development of composite civil aircraft. Proceedings of the "16th National Journeys on Composites (JNC16)" (2009)
30. Collombet, F., Luyckx, G., Sonnenfeld, C., Grunevald, Y.H., Davila, Y., Torres, M., Jacob, X., Wu, K.T., Rodriguez, S., Douchin, B., Crouzeix, L., Bazer-Bachi, R., Geernaert, T., Degrieck, J., Berghmans, F.: Cure monitoring of an autoclave manufactured industrial part: added value of complementary instrumentation. Proceedings of the "19th International Conference on Composite Materials". 2013.
31. Sonnenfeld, C., Luyckx, G., Collombet, F., Grunevald, Y.H., Douchin, B., Crouzeix, L., Torres, M., Geernaert, T., Sulejmani, S., Chah, K., Mergo, P., Thienpont, H., Berghmans, F.: Cure cycle monitoring of laminated carbon fiber-reinforced plastic with fiber Bragg gratings in microstructured optical fiber. Proceedings of the "19th International Conference on Composite Materials" (2013)
32. Torres, M., Collombet, F., Douchin, B., Crouzeix, L., Bazer-Bachi, R., Grunevald, Y.-H., Lubin, J., Camps, T., Jacob, X., Rodriguez, S., Wu, K.-T.: Monitoring of the curing process of an industrial composite structure by TJS and FUT, Proceedings of the "35th International Conference on Metallurgy and Materials" (2013)